organics

MDPI

Article

Diastereomeric *N,S*-Dialkyl Dithiocarbamates Derived from (*E*)-Chalcones and L-Tryptophan: Microwave-Assisted Synthesis and In Vitro Studies Against *Fusarium oxysporum*

Natalia Agudelo-Ibañez, Sergio Torres-Cortés, Ericsson Coy-Barrera, Ivon Buitrago and Diego Quiroga *

Bioorganic Chemistry Laboratory, Facultad de Ciencias Básicas y Aplicadas, Universidad Militar Nueva Granada, Cajicá 250247, Colombia; u0500892@unimilitar.edu.co (N.A.-I.); sergio.torres@unimilitar.edu.co (S.T.-C.); ericsson.coy@unimilitar.edu.co (E.C.-B.); ivon.buitragov@unimilitar.edu.co (I.B.)
* Correspondence: diego.quiroga@unimilitar.edu.co

Abstract: The synthesis of indole phytoalexin-like analogs related to alkyl (((1-(4-substitutedphenyl)-3-oxo-3-phenylpropyl)thio)carbonothioyl)-L-tryptophanate **1a–d** and the evaluation of their antifungal activity against the phytopathogen *Fusarium oxysporum* is reported. The target compounds were synthesized in the following two stages: (1) the initial esterification of L-tryptophan, which reacted with trimethyl silane chloride and simple aliphatic alcohols (R = Me, Et) under microwave irradiation (MWI) at 100 °C to obtain the respective alkyl ester **2a–b**; (2) the resulting mixture of L-tryptophanates **2a–b** with carbon disulfide and (*E*)-chalcone **3a–b** under MWI at 50 °C during 60 min, followed by purification through classical column chromatography (55–76% yields). The products were obtained as mixtures of (*S,R)* and (S,*S*) diastereoisomers. An LC-DAD-MS analysis allowed us to establish the ratio of these diastereoisomers, and subsequent DFT/B3LYP-based computational calculations of the NMR ^{1}H chemical shifts suggested that the major diastereoisomer involved an (*S,R*) absolute configuration, comprising more than 60% of the mixture. The compounds **1a–d** were subjected to an antifungal activity test against the phytopathogen *F. oxysporum* using an amended medium-based assay. Compound series **1** showed inhibition percentages of 80% at the first concentration and IC_{50} values between 0.33 and 5.71 mM, demonstrating greater potential as antifungal agents compared to other L-tryptophan derivatives like alkyl (2*S*)-3-(1*H*-indol-3-yl)-2-{[(1*Z*)-3-oxobut-1-en-1-yl]amino}propanoate, which presented lower inhibition percentages. In summary, phytoalexin analogs derived from L-tryptophan and (*E*)-chalcones significantly inhibited the mycelial growth of *Fusarium oxysporum*, indicating their potential as effective antifungal agents.

Keywords: L-tryptophan derivatives; chalcone derivatives; indolic phytoalexin; microwave-assisted synthesis; *Fusarium oxysporum*

Citation: Agudelo-Ibañez, N.; Torres-Cortés, S.; Coy-Barrera, E.; Buitrago, I.; Quiroga, D. Diastereomeric *N,S*-Dialkyl Dithiocarbamates Derived from (*E*)-Chalcones and L-Tryptophan: Microwave-Assisted Synthesis and In Vitro Studies Against *Fusarium oxysporum*. *Organics* **2024**, *5*, 598–613. https://doi.org/10.3390/org5040031

Academic Editors: Tomasz K. Olszewski and Wim Dehaen

Received: 12 August 2024
Revised: 22 November 2024
Accepted: 4 December 2024
Published: 9 December 2024

1. Introduction

Dialkyl dithiocarbamates are a group of organic nitrogen–sulfur compounds widely studied for their versatility and ease of synthesis by employing amines, carbon disulfide, and electrophilic reagents as precursors [1]. Its behavior as a vulcanization accelerator; foam flotation collector; antifouling; coatings; lubricant additives [2]; the interaction of their mercury (II) complexes with anions, leading to pseudopolymeric Au(III)–heteronuclear complexes Hg(II), which, through thermolysis, leads to the quantitative regeneration of the bound gold and the subsequent release of $HgCl_2$ as HgS [3]; and the photocatalytic properties of some ruthenium complexes [4] have demonstrated their importance for the design of novel materials. However, their biological properties have also been reported. Arylsulfonyl-*N*,*N*-dialkyl-dithiocarbamates were designed and obtained to evaluate their reactivity against a cysteine residue of the heterodimeric protein tubulin, since many antitumor drugs exert their action by binding to tubulin, inhibiting the association of microtubules

and causing cell death. Arylsulfonyl-*N*,*N*-dialkyl-dithiocarbamates substituted with 4-halogen, 4-methyl-, or 4-carboxyphenyl acted as tubulin polymerization inhibitors [5]. Gold(I) complexes containing tri-*tert*-butylphosphine and dialkyl dithiocarbamate ligands showed in vitro cytotoxicity against the human cancer cell lines A549 (lung cancer), MCF7 (breast cancer), and HeLa (cervical cancer) [6]. These results suggested that the (C=S)-S group may behave as a potential pharmacophore and could be responsible for the reported biological activities.

The dithiocarbamate function is present in several secondary metabolites, such as brassinin, a phytoalexin identified for the first time as a constituent of cabbage, which has been studied due to its cancer chemopreventive activity [7]. The bifunctional structural nature of brassinin, characterized by the presence of an indole nucleus and a dithiocarbamoyl-aminomethyl moiety, is remarkably similar to the individual structural elements of other known chemopreventive agents such as indole-3-carbinol or benzyl isothiocyanate. Their demonstrated favorable biological activity is attributed to the presence of these two residues. Further studies have revealed that brassinin could be a moderate inhibitor of indoleamine 2,3-dioxygenase (IDO), a protoleragenic enzyme that drives immune escape in several types of cancer, since the dithiocarbamate moiety can bind the iron heme group of IDO. Substituting the *S*-methyl group of brassinin with large aromatic groups provides inhibitors that are, presumably, three times more potent than the most commonly used IDO inhibitors [8,9]. The behavior as a bioavailable inhibitor of IDO of the synthetic derivative 5-bromo-brassinin was also demonstrated [10]. Moreover, the antifungal effect of brassinin against different species of *Alternaria* has also been proved, showing a remarkable influence on the germ tube elongation, conidial germination, and mycelial growth of the phytopathogen [11].

These backgrounds have inspired our research towards the synthesis of bioactives based on novel bioisosteres of brassinin derived from L-tryptophan. We have developed an efficient methodology to synthesize novel antifungal brassinin analogs from L-tryptophan such as *N*,*N*′-dialkylthioureas, 4-[(1*H*-indol-3-yl)methylene]-2-sulfanylidene-1,3-thiazolidin-5-ones, and alkyl (2*S*)-3-(1*H*-indol-3-yl)-2-{[(alkylsulfanyl)carbonothioyl]amino} propanoates via a tandem dithiocarbamate formation–Michael addition reaction. The evaluation of the antifungal activity of these products against *Fusarium oxysporum* allowed us to establish that this class of derivatives can show promise as antifungal agents [12]. Furthermore, we have described a rapid, green, high-yield synthesis of these compounds using ultrasonic irradiation in water. The L-alanine, L-phenylalanine, and L-tyrosine derivatives were tested for their antifungal activity against *F. oxysporum*, and some showed the effective inhibition of mycelial growth, demonstrating that sterically bulky electron-withdrawing groups enhance the inhibitory action [13]. Inspired by these facts, a subsequent in silico study allowed us to extend our scope to employ more biologically valuable Michael acceptors such as (*E*)-chalcones, a versatile and profitable group of compounds broadly known in the literature for its biological activities [14]. The in silico results in this previous study suggested that sterically bulky and electron-rich substituents are crucial for increasing mycelial growth inhibition. In addition, the evaluated compounds, which were proposed as derivatives from (*E*)-chalcone and L-tryptophan, showed a specific interaction mode involving non-polar electrostatic interactions with lanosterol 14α-demethylase (LDM) [15]. The 3D-QSAR model obtained by a comparative molecular field analysis (CoMFA) was conducted to understand the antifungal activity of the diastereoisomers (S,*R*) of alkyl (((3-oxo-1,3-diphenylpropyl)thio)carbonothioyl)-L-tryptophanate (Figure 1), which showed promissory results by molecular docking calculations. This CoMFA analysis revealed that the antifungal activity is significantly influenced by both electrostatic (35.3%) and steric (29.2%) factors. Notably, these compounds exhibited potential antifungal properties, attributed to their favorable interactions with key residues in LDM, a critical enzyme in fungal sterol biosynthesis. Additionally, molecular dynamics simulations revealed that the complex with *Fc*LDM maintained structural stability, with non-polar interactions identified as the primary driving force for the binding, highlighting their potential as promising antifungal agents. This outcome was also rationalized, since it is widely known that

(*E*)-chalcones and derived moieties exhibit biological activities, such as anti-inflammatory activities [16] and antifungal activities, against *Phomopsis sp.* [17], *Plasmodium falciparum* [18], *Rhizoctonia solani* [19], and *Cryptococcus neoformans* [20].

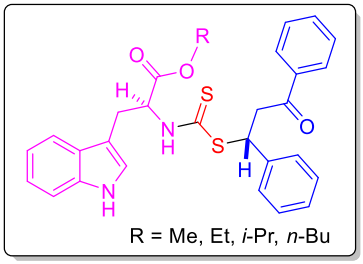

Figure 1. Chemical structure of the (*S*,*R*)-diastereoisomers of alkyl (((3-oxo-1,3-diphenylpropyl) thio)carbonothioyl)-L-tryptophanates previously analyzed [15].

Thus, through the integration of computational methods, such as CoMFA, molecular docking, and molecular dynamics, the rational design of effective antifungal compounds paved the way for the exploration and optimization of this promising lead. For this reason, we explore the synthesis of additional analogs and, subsequently, the validation of their biological activity against *Fusarium oxysporum*. The synthesis and the in vitro antifungal activity evaluation against *F. oxysporum* of new dithiocarbamates related to alkyl (((1-(4-substitutedphenyl)-3-oxo-3-phenylpropyl)thio)carbonothioyl)-L-tryptophanate **1a**–**d**, obtained from L-tryptophan and the 4-substituted (*E*)-chalcones **3a**–**b** (R = Cl, OH), is discussed. The results obtained are described below. The findings support the concept that these indole-containing phytoalexin-based bioisosteres could be potential agrochemical agents for controlling *Fusarium* spp. phytopathogens.

2. Materials and Methods

2.1. General Information

All of the reagents and chemicals were purchased commercially (Merck KGaA and/or Sigma-Aldrich, Darmstadt, Germany). They were employed without further purification. As a result, the purity of the dry solvents was sufficiently defined during the purchase. The progression of the reactions and purifications of the products was monitored by thin-layer chromatography (TLC) on silica gel 60 F254 plates (Merck KGaA) under detection at 254 nm. Nuclear magnetic resonance (NMR) experiments were performed using a Bruker Avance AV-400 MHz spectrometer. TMS was used as a reference for chemical changes in δ (ppm). Typical splitting patterns were implemented to define the multiplicity of the signal (i.e., *s*, singlet; *d*, doublet; *t*, triplet; *m*, multiplet). Gas chromatography–mass spectrometry (GC/MS) analysis of compound **1a** was performed on a Trace 1300 LT gas chromatograph (Thermo Scientific, Waltham, MA, USA) coupled to a Thermo ISQ mass spectrometer, and equipped with electron impact ionization and a single quadrupole analyzer. The sample was injected at a concentration of 5 mg/mL in splitless mode, and the injection port temperature was set at 300 °C. Analytes were separated using a high-temperature capillary column (60 m × 0.25 mm ID × 0.25 µm Rxi® 5 Sil MS, Restek, State College, PA, USA). Helium (99.999%) was used as carrier gas at 1.5 mL/min. The temperature program was initially held at 100 °C for 1 min, and then increased from 100 °C to 250 °C at 15 °C/min and held at 250 °C for 5 min. Finally, the program was increased from 10 °C/min to 310 °C and held at 310 °C for 30 min. The compounds were detected and separated in the total ion chromatogram (TIC) and were identified using the diagnostic fragments observed in the electron impact-derived mass spectra. High-performance liquid chromatography (HPLC) coupled to mass spectrometry (MS) analyses were performed from the crude reaction mixtures. The chemical reactions were carried out in a Discover System microwave reactor model 908.005 series DY1030 in a closed container, controlling the temperature.

2.2. Chemical Synthesis of Compounds

Alkyl esters derived from L-tryptophan **2a**–**b** were prepared under microwave irradiation, mixing the reagents in the following order: L-tryptophan (1 mmol) with TMSCl (4 mmol) and the respective alcohol (R = Me, Et; 1 mL). First, the mixture was heated at 100 °C for 10 min under microwave irradiation in a closed atmosphere. Then, in the same microwave tube, Et_3N (4 mmol), carbon disulfide (1 mL), and the respective 4-substituted (*E*)-chalcone (R = Cl, OH) **3a**–**b** (1 mmol) were added. The reaction mixture was further heated at 50 °C for 60 min under microwave irradiation. The progress of the reaction was followed by thin-layer chromatography (TLC) until no reactants were detected. Then, the solvent was removed by vacuum distillation. Finally, the products **1a**–**d** were obtained by column chromatography eluting with petroleum ether/ethyl acetate mixtures.

2.2.1. Methyl (((1-(4-Chlorophenyl)-3-oxo-3-phenylpropyl)thio)carbonothioyl)-L -tryptophanate (**1a**, $C_{28}H_{25}ClN_2O_3S_2$)

Yellowish oil; ^{1}H NMR (400 MHz, $CDCl_3$) δ: 8.21 (*s*, 2H), 7.53 (*dd*, *J* = 7.7, 4.0 Hz, 2H), 7.34 (*d*, *J* = 8.1 Hz, 2H), 7.22–7.08 (*m*, 2H), 6.96 (*m*, 3H), 6.76 (*d*, *J* = 7.7 Hz, 1H), 5.25 (*m*, 1H for (*S*,*R*) diastereoisomer), 4.89–4.75 (*m*, 1H for (*S*,*S*) diastereoisomer), 4.13 (*m*, 1H), 3.94 (*s*, 3H), and 3.55–3.24 (*m*, 4H); ^{13}C NMR (100 MHz, $CDCl_3$) δ: 192.1, 169.2, 167.2, 136.1, 136.0, 128.2, 127.6, 127.0, 125.9, 124.2, 123.3, 122.2, 119.7, 118.8, 118.7, 118.7, 115.9, 112.8, 112.1, 111.3, 110.7, 60.6, 57.9, 53.0, 31.1, and 24.0. GC-MS: total ion chromatogram (TIC) at the following three retention times: 18.1 min (*m*/*z* 242.19 [M-$C_{13}H_{16}N_2O_2S_2$]), 18.7 min (*m*/*z* 276.18 [M-$C_{13}H_{13}N_2O_2S$]), and 19.1 min (*m*/*z* 260.17 [M-$C_{15}H_{12}ClOS$]). ESI$^+$-MS *m*/*z* [M + H]$^+$, 538; [M + MeOH + H]$^+$, 570.

2.2.2. Ethyl (((1-(4-Chlorophenyl)-3-oxo-3-phenylpropyl)thio)carbonothioyl)-L -tryptophanate (**1b**, $C_{29}H_{27}ClN_2O_3S_2$)

Yellowish oil; ^{1}H NMR (400 MHz, $CDCl_3$) δ_H: 8.22 (*s*, 2H), 7.54 (*d*, *J* = 7.6 Hz, 2H), 7.34 (*d*, *J* = 8.1 Hz, 2H), 7.20–7.03 (*m*, 5H), 6.98 (*d*, *J* = 2.3 Hz, 2H), 6.74 (*d*, *J* = 7.8 Hz, 1H), 5.24 (*m*, 1H for (*S*,*R*) diastereoisomer), 4.79 (*m*, 1H for (*S*,*S*) diastereoisomer), 4.56–4.40 (*q*, *J* = 7.1 Hz, 2H), 4.17–4.07 (*m*, 1H), 3.36 (*m*, 4H), and 1.30 (*t*, *J* = 7.1 Hz, 3H); ^{13}C NMR (100 MHz, $CDCl_3$) δ_C: 190.0, 171.4, 170.6, 136.2, 136.1, 127.7, 127.2, 123.4, 122.9, 122.3, 122.2, 119.7, 119.7, 118.7, 118.4, 111.4, 111.2, 109.8, 109.2, 66.7, 61.7, 58.2, 28.4, 27.0, and 14.1. ESI$^+$-MS *m*/*z* [M + H]$^+$, 552; [M + MeOH + H]$^+$, 584.

2.2.3. Methyl (((1-(4-Hydroxyphenyl)-3-oxo-3-phenylpropyl)thio)carbonothioyl)-L -tryptophanate (**1c**, $C_{28}H_{26}N_2O_4S_2$)

Yellowish oil; ^{1}H NMR (400 MHz, $CDCl_3$) δ_H: 8.41 (*s*, 2H), 8.06–7.92 (*m*, 1H), 7.62–7.48 (*m*, 1H), 7.25–7.10 (*m*, 9H), 6.89 (*d*, *J* = 8.6 Hz, 1H), 5.58 (*m*, 1H for (*S*,*R*) diastereoisomer), 4.58 (*m*, 1H for (*S*,*S*) diastereoisomer), 4.15 (*m*, 1H), 3.75 (*s*, 3H), and 3.50–3.29 (*m*, 4H); ^{13}C NMR (100 MHz, $CDCl_3$) δ_C: 191.4, 171.7, 169.0, 145.6, 136.2, 133.3, 130.6, 128.7, 128.5, 128.3, 126.9, 124.2, 122.3, 119.8, 118.3, 116.2, 115.6, 111.6, 108.9, 60.7, 60.3, 53.3, 45.4, and 30.1. ESI$^+$-MS *m*/*z* [M + H]$^+$, 520; [M + MeOH + H]$^+$, 552.

2.2.4. Ethyl (((1-(4-Hydroxyphenyl)-3-oxo-3-phenylpropyl)thio)carbonothioyl)-L -tryptophanate (**1d**, $C_{29}H_{28}N_2O_4S_2$)

Yellowish oil; ^{1}H NMR (400 MHz, $CDCl_3$) δ_H: 8.16 (*s*, 2H), 8.00–7.90 (*m*, 1H), 7.55–7.30 (*m*, 5H), 7.22–7.00 (*m*, 5H), 6.70 (*d*, *J* = 8.5 Hz, 1H), 5.24 (*m*, 1H for (*S*,*R*) diastereoisomer), 4.49 (*m*, 1H for (*S*,*S*) diastereoisomer), 4.19–4.06 (*m*, 1H), 4.51–4.40 (*q*, *J* = 7.1 Hz, 2H), 3.57–3.23 (*m*, 4H), and 1.30 (*t*, *J* = 7.1 Hz, 1H); ^{13}C NMR (100 MHz, $CDCl_3$) δ_C: 190.1, 171.5, 170.7, 136.2, 133.3, 130.6, 128.8, 128.3, 127.9, 123.4, 123.0, 122.4, 119.8, 118.9, 118.5, 116.2, 115.6, 111.3, 110.0, 66.8, 61.7, 58.3, 45.4, 27.1, and 14.3. ESI$^+$-MS *m*/*z* [M + H]$^+$, 534; [M + MeOH + H]$^+$, 566.

2.3. HPLC-MS Analysis

The chemical profiles of the resulting diastereoisomeric mixtures **1a–d** were analyzed using reverse-phase (RP) liquid chromatography (LC) coupled with mass spectrometry (MS). A Prominence ultra-fast LC system (Shimadzu, Columbia, MD, USA) was employed, equipped with a photodiode array detector (DAD) and a Shimadzu LCMS 2020 mass spectrometer (Shimadzu, Columbia, MD, USA) featuring a quadrupole analyzer and electrospray ionization (ESI). Separation was carried out on a Kinetex C18 column (150 × 4.6 mm, 2.6 µm) (Phenomenex, Torrance, CA, USA), using a 10 µL sample injection and eluted with a program using solvent A (Type-I water) and B (MS-grade methanol). The gradient elution method started with 0–1 min of 30% B, 1–7 min from 30% to 60% B, 7–12 min from 60% to 95% B, 12–16 min 95%, and 16–18 min from 95% to 30% B. DAD was configured for monitoring at 280 nm. Mass spectra were simultaneously acquired using ESI in the positive ion mode (scan 100–2000 m/z). The MS parameters involved a voltage detector at 1.5 kV, a curved desolvation line at 250 °C, a heat block temperature of 400 °C, and a nebulization gas flow of 1.5 L/min.

2.4. Antifungal Assay

The compounds **1a–b** were evaluated against *F. oxysporum* following the previously reported 12-well plate-modified medium method to evaluate the in vitro inhibition of mycelial growth [21]. For this study, a strain of *Fusarium oxysporum* was used, and it was recovered from a diseased *Physalis peruviana* plant. The IC_{50} values were calculated from the log(dose) versus mycelial growth inhibition curves by nonlinear regression using GraphPad Prism 9.0 for Windows.

2.5. DFT-B3LYP Computational Calculations

Theoretical calculations were performed using the PC Spartan'14 software (Wavefunction Inc., Irvine, CA, USA). The NMR spectra and geometric structure of compounds **1c–d** were fully optimized without imposing any symmetry constraint with Becke's three-parameter hybrid functional and the Lee–Yang–Parr correlation functional (B3LYP) at the level 6-311G*.

3. Results and Discussion

The 4-substituted (*E*)-chalcones **3a–b** were previously obtained from the Claisen–Schmidt reaction using a method previously reported in the literature [22]. Once the 4-substituted (*E*)-chalcones **3a–b** were obtained, the reaction between this type of precursor, carbon disulfide, and the alkyl esters **2a–b** [23] was carried out. Initially, the methodology proposed by Quiroga et al. [12] was employed, which involves reacting the precursors through a tandem reaction strategy that includes the formation of a dithiocarbamate-type ionic intermediate followed by a Michael addition reaction. To this end, the respective alcohols (R = Me, Et), trimethylsilane chloride, and triethylamine were added to a solution of L-tryptophan in THF. Subsequently, a solution of carbon disulfide and the corresponding (*E*)-chalcone was added dropwise. The reaction mixture was stirred at room temperature for 24 h and then concentrated under reduced pressure. However, in all cases, the starting (*E*)-chalcone was recovered, and no reagent consumption was observed. These results suggest that the reactivity of (*E*)-chalcone type compounds is lower than that of Michael acceptors such as acrylonitrile, mesityl oxide, and methyl acrylate, which reacted at room temperature. Even exposing the reaction mixture to ultrasound irradiation (US) under the same conditions proved unsuccessful. A recent study by Kenari et al. [24] indicates that the Michael reaction involving (*E*)-chalcones, which is typically base-catalyzed, depends on the charge of the nucleophilic reagents. These can be negatively charged (e.g., OH^-, RS^-, and CN^-) or neutral (e.g., amines and thiols). Kenari stated that the primary adducts of the addition reactions may either possess a negative charge (when involving charged nucleophiles) or adopt a zwitterionic structure (when involving neutral nucleophiles). In the second step of the reaction, acid–base interactions occur either in an intermolecular in-

termediate or, in the case of the zwitterionic intermediates, intramolecularly. This suggests that the acid–base character of the medium could influence the progression of the reaction. Furthermore, several reports have indicated that this class of compounds reacts more favorably at higher temperatures than room temperature [25–27]. For instance, Al-Jaber et al. [27] reported the Michael addition reaction of 1,3-diphenylpropenone with *o*-aminothiophenol in the presence of indium trichloride, yielding benzothiazine derivatives under reflux.

Considering the described antecedents, we employed a methodology through the following two stages: (1) the synthesis of alkyl esters derived from L-tryptophan according to the Li and Sha protocol [23] with a quantitative performance; (2) the reaction of the in situ-formed alkyl esters **2a**–**b**, with each precursor **3a**–**b** and carbon disulfide under microwave irradiation, and the use of trimethylamine (TEA) as a basic catalyst (Scheme 1). Monitoring the reaction using thin-layer chromatography (TLC) using silica gel as the stationary phase and a mixture of hexane/ethyl acetate (80:20) as the mobile phase allowed us to detect the reagent consumption. The formation of the products **1a**–**d** was detected after 60 min.

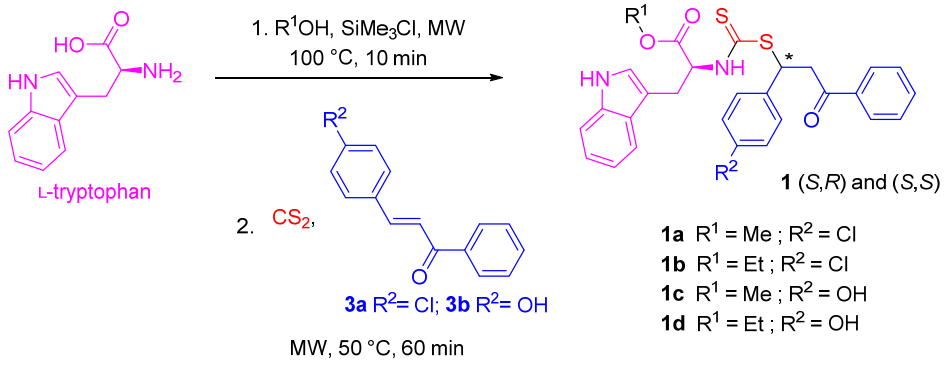

Scheme 1. Synthesis of compounds **1a**–**d** from L-tryptophan and 4-substituted (*E*)-chalcones **3a**–**b**.

As we mentioned previously, it is expected that the reaction between the dithiocarbamate intermediate derived from L-tryptophan and the 4-substituted (*E*)-chalcone leads to the formation of a new chiral center that is additional to that coming from the amino acid with the *S* configuration. The reaction mixture for the formation of compound **1a** was analyzed by 1H NMR (Figure S1). This mixture comprises the precursors L-tryptophan, carbon disulfide, and *trans*-4-chlorochalcone **3a**. Among these, only the methyl ester of L-tryptophan is expected to show signals between 3.0 and 6.0 ppm. Specifically, this ester should exhibit one multiplet for the hydrogen on the carbon attached to the chiral center, two doublets for the diastereotopic benzylic hydrogens, and one singlet for the methyl group CH_3O. Upon reaction with carbon disulfide, this ester forms an ionic dithiocarbamate intermediate (a nucleophile), which likely undergoes a Michael addition to the chalcone. This reaction introduces a new set of hydrogens, which we expect to appear between 3.0 and 6.0 ppm: two multiplets for hydrogens on the carbon adjacent to the carbonyl group and one multiplet for the hydrogen on the newly formed chiral center (*S* or *R*). These signals appear in the raw spectrum (blue trace), although complex due to the diastereomeric mixture. Additional spectra correspond to the purified diastereomers of 1a (dark red traces), achieved by MPLC purification, although only compound 1a was isolated entirely; compound 1b showed degradation during the purification process. When comparing the diastereomers, the main distinction lies in the multiplet between 4.50 and 4.70 ppm and the signal between 5.10 and 5.30 ppm. Based on our analysis, the signal at 4.50–4.70 ppm was assigned to the (*S*,*S*) diastereomer, and the signal at 5.10–5.30 ppm was assigned to the (*S*,*R*) diastereomer. The signal in question, a singlet at 3.70 ppm, is observed in the spectrum of the (*S*,*R*) diastereomer. However, this signal also appears in the spectrum of the (*S*,*S*) diastereomer (Figure S2), albeit slightly shifted to 3.75 ppm, with an identical multiplicity.

To establish the ratio of diastereoisomers (*S*,*R*)- and (*S*,*S*)-**1a**–**d**, the reaction crudes were subjected to reverse-phase HPLC-DAD-MS analysis (Figure 2) under mild elution conditions so to avoid in-column degradation. The wavelength used to detect compounds **1a**–**d** was 280 nm, the typical maximum absorption of dihydrochalcones [28], simultaneously to the MS detection. The HPLC-DAD-MS-based chemical profiles revealed that products **1a** and **1b**, derived from (*E*)-4-chlorochalcone, exhibited two distinct signals with retention times (RTs) within 10–13 min for **1a** and 13–15 min for **1b**, both displaying similar intensities and areas in the chromatogram. Using the ESI detector in positive ion mode, we identified corresponding signals for the adducts $[M + H]^+$ and $[M + MeOH + H]^+$, which showed identical values (Figure S8). Compounds **1c** and **1d**, derived from (*E*)-4-hydroxychalcone, yielded results comparable to those of compounds **1a** and **1b**. This analysis confirmed the presence of two possible diastereoisomers, i.e., (*S*,*R*) and (*S*,*S*), formed through the Michael reaction to obtain the target *N*,*S*-dialkyl dithiocarbamates. Although the identity of individual chromatographic signals could not be definitively assigned to each diastereoisomer, we inferred that the (*S*,*S*)-diasteroisomer is likely more polar than the (*S*,*R*)-diasteroisomer based on the DFT-calculated dipole moments (5.12–5.14 D for (*S*,*S*) vs. 1.11–1.24 D (*S*,*R*)), respectively), which explained the RP-LC performance (i.e., a lower RT for (*S*,*S*) and higher RT for (*S*,*R*)). Additionally, this analysis enabled us to determine the diastereomeric ratio for each target compound (**1a**–**d**), as summarized in Table 1, involving a diastereomeric excess [(*S*,*R*)–(*S*,*S*)] of ca. 7% and 13% for (*E*)-4-chlorochalcone- and (*E*)-4-hydroxychalcone-derived *N*,*S*-dialkyl dithiocarbamates, respectively (**1a**–**b** and **1c**–**d**).

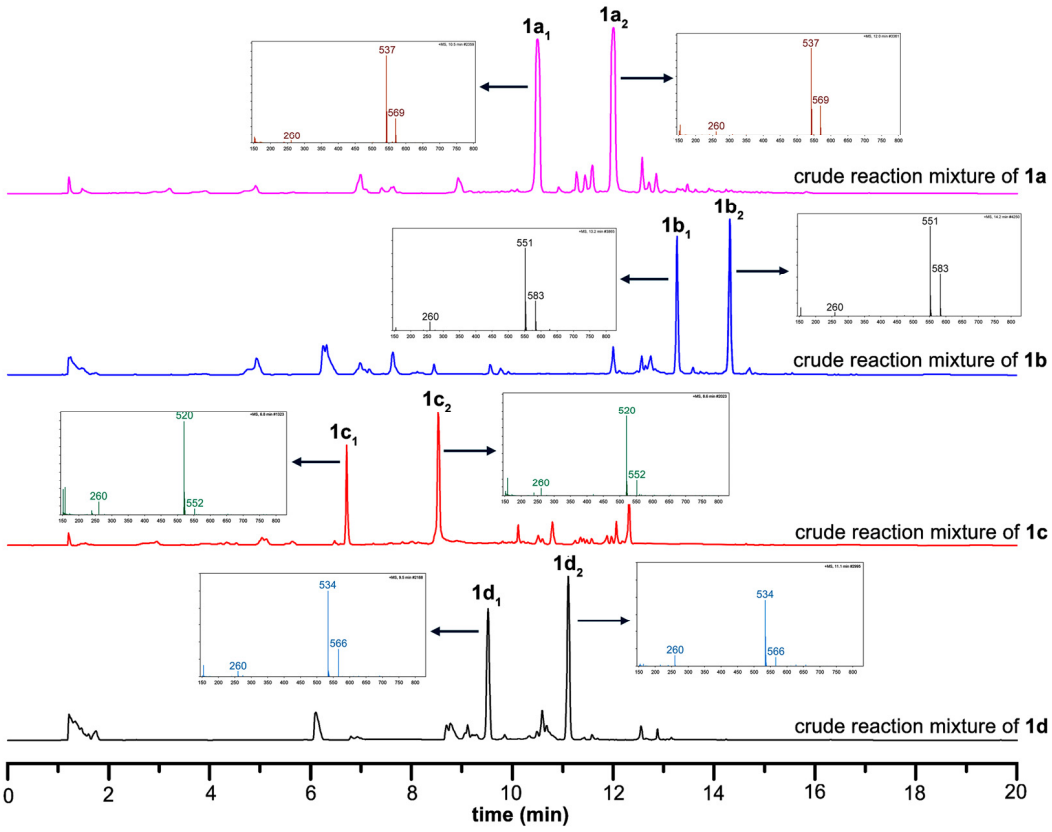

Figure 2. Chromatographic profiles for the crude reaction mixtures obtained after the synthesis of compounds **1a**–**d**. Lowercase numbers for each signal assignment (i.e., $\mathbf{1a_1}$–$\mathbf{d_1}$ and $\mathbf{1a_2}$–$\mathbf{d_2}$) indicate the discrimination of two diastereoisomers ((*S*,*S*) or (*S*,*R*)). Each plot pinpointed to a specific diastereoisomer corresponds to its respective mass spectrum, which displays *m*/*z* signals for the ESI-MS adducts $[M + H]^+$ (the more intense MS signal) and $[M + MeOH + H]^+$ (lesser intense, final MS signal).

Table 1. Yield percentages and diastereomeric ratio for compounds **1a–d**.

Compound	R^{1} [a]	R^{2} [a]	Yield (%) [b]	Diastereomeric (*S*,*S*/*S*,*R*) Ratio (%) [c]
1a	Me	Cl	76	46.6/53.3
1b	Et	Cl	69	45.8/54.2
1c	Me	OH	58	43.4/56.6
1d	Et	OH	56	42.9/57.1

[a] Substituents (R^{1} and R^{2}) as depicted in Scheme 1; [b] Yields corresponding to the column chromatography-depurated diastereomeric mixtures; [c] Determined by HPLC-DAD analysis.

To achieve the separation of the (*S*,*R*)-diastereomers, which have the potential as antifungal agents against *Fusarium oxysporum* [28], and to facilitate the subsequent structural elucidation, classical column chromatography was employed. However, the high structural similarity and comparable chromatographic behavior of the diastereomers limited an effective separation under these classical conditions. The yield obtained from the diastereomeric mixtures ranged from 56% to 76% (Table 1). Attempts to utilize other purification techniques, such as recrystallization, precipitation, or sublimation, were unsuccessful, resulting in the noticeable degradation of the products. Consequently, structural elucidation was conducted using the diastereomeric mixtures. The analysis by nuclear magnetic resonance (NMR) is detailed below, incorporating both one- and two-dimensional experiments.

The ^{1}H NMR spectra of compounds **1a–d** (Figures S3a–S6a) present several characteristic signals that allow for their adequate characterization. Firstly, a group of signals overlapping each other is observed, between 3.60 and 3.20 ppm, which appear as double doublets and multiplets. These signals were assigned to the methylene groups adjacent to chiral carbons, which are found both in the fragment from the ester group and the one resulting from the binding between the dithiocarbamate fragment and the (*E*)-chalcone. The signals between 6.75 and 8.25 ppm correspond to the hydrogen atoms of the aromatic rings in both of the phenyl groups and the indole fragment of the molecule. A singlet signal at 3.97 ppm was assigned to the methyl group of the ester, which should integrate for three hydrogen atoms. Multiplets with an integration area of one hydrogen atom around 4.12 and 5.24 ppm were observed and assigned to the proton directly attached to each chiral center. However, a low-area multiplet signal (0.42) was also detected at 4.85 ppm, presumably corresponding to a hydrogen atom directly attached to a chiral center. The new asymmetric center can have an *S* or *R* configuration that promotes the formation of two diastereoisomers having (*S*,*R*) or (*S*,*S*) configurations, which explains the presence of the mentioned multiplets. Furthermore, the areas of the remaining signals, although they are close to the expected value according to the assignment, are not actually integer values, which suggests the overlapping of the spectra of each diastereoisomer.

With the aim of differentiating the formed diastereoisomers and trying to identify the major instances of them due to the unsuccessful classic chromatographic separation, we calculated the ^{1}H and ^{13}C NMR spectra of each diastereoisomer using the DFT/B3LYP method. Density functional theory (DFT) has proven to be an invaluable tool for predicting NMR chemical shifts and correlating them with experimental data. The accuracy of these predictions depends on the choice of functionals and basis sets, and DFT calculations provide significant advantages for studying complex molecular systems. Venianakis et al. [29] demonstrated the utility of the DFT method in predicting the NMR chemical shifts of conjugated linoleic acids, showing that ^{1}H NMR shifts offer a high discrimination capacity between geometrical isomers, with results that align well with the experimental data even at lower levels of theory. Furthermore, they reported that the B3LYP/6-311++G(d,p) level yields excellent linear correlations between the calculated and experimental data, and can be used to obtain detailed information on the 3D structure of molecules in solution, demonstrating the robustness of the method across different functionals. The accuracy of DFT in predicting the ^{1}H NMR chemical shifts for conjugated trienyl compounds was determined [30], achieving excellent agreement with experimental data. Steric interactions between closely spaced olefinic protons were well reproduced by DFT calculations, further

validating its role in structural elucidation. In cases where experimental resonance assignments were ambiguous due to signal overlap, DFT calculations were pivotal in resolving these issues. Recently, Safi and Wazzan [31] conducted an analysis comparing the accuracy of various functionals in predicting both ^{1}H and ^{13}C NMR chemical shifts in azo dyes. Their findings indicate that geometry optimization is crucial for accurate NMR predictions, particularly for ^{1}H NMR shifts. Considering this background and the high accuracy of DFT calculations in predicting NMR chemical shifts when appropriate functionals and basis sets are employed, we propose using this tool to differentiate the diastereomers formed. The results are depicted in Figure 3.

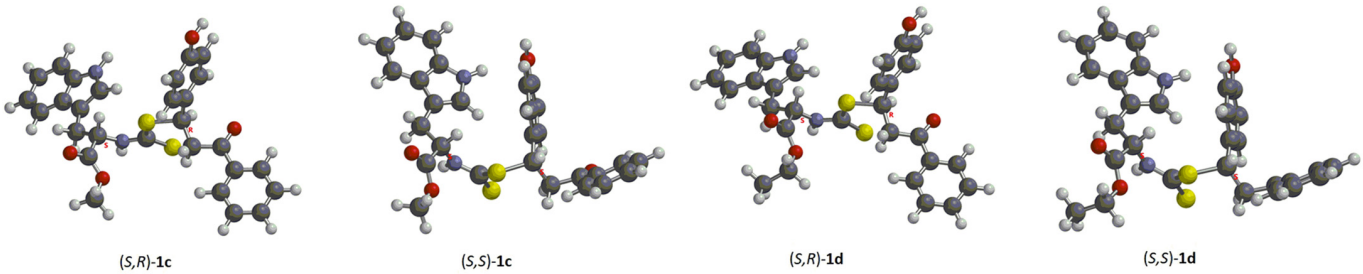

(a)

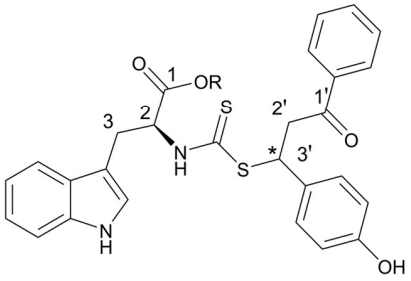

(b)

	1c			1d		
Label	Exp.	(S,S) Caltd.	(S,R) Caltd.	Exp.	(S,S) Caltd.	(S,R) Caltd.
H2	4.13	4.60	4.76	4.13	4.57	4.68
H3a	3.40	3.44	3.34	3.39	3.48	3.27
H3b	3.42	2.63	2.88	3.41	2.64	2.92
H2a'	3.39	3.66	3.44	3.40	3.66	3.40
H2b'	3.43	4.76	3.72	3.42	4.75	3.76
H3'	5.58	4.45	5.26	5.24	4.42	5.25
C2	60.3	59.9	56.8	58.3	59.9	57.2
C3	30.1	28.6	30.1	27.1	28.5	29.9
C2'	45.4	41.0	43.8	45.4	41.2	44.0
C3'	60.6	55.0	63.2	61.7	54.7	63.1

Figure 3. (**a**) DFT-derived models for diastereomers of compounds **1c**–**d**; (**b**) ^{1}H and ^{13}C calculated chemical shift for the diastereoisomers (*S*,*R*)-**1c**, (*S*,*S*)-**1c**, (*S*,*R*)-**1d**, and (*S*,*S*)-**1d**.

The comparative analysis of the computational properties of the (*S*,*S*) and (*S*,*R*) diastereomers of compound **1c** reveals key differences in the energy, dipole moment, and energy levels of the HOMO and LUMO orbitals, which may affect their reactivity and stability. The (*S*,*R*) diastereomer is slightly more stable, as it exhibits a lower (more negative) energy than the (*S*,*S*). Although the energy difference is small (0.00736 au), this additional stability may influence its predominance under certain conditions. The dipole moment of (*S*,*S*)-**1c** is significantly higher than that of (*S*,*R*)-**1c**. The HOMO energy of (*S*,*R*)-**1c** is lower than that of (*S*,*S*)-**1c**, indicating that (*S*,*R*)-**1c** has a lower capacity to donate electrons, i.e., it is less reactive in electron transfer reactions from the HOMO. The LUMO energy of (*S*,*R*)-**1c** is higher than that of (*S*,*S*)-**1c**, suggesting that (*S*,*R*)-**1c** might be less receptive to accepting electrons, i.e., less electrophilic compared to (*S*,*S*). The HOMO-LUMO gap of (*S*,*R*)-**1c** is higher than that of (*S*,*S*)-**1c**, indicating that, presumably, (*S*,*R*)-**1c** might be more chemically stable but less reactive. Diastereoisomers of compound **1d** showed similar results, where the (*S*,*R*) diastereomer is slightly more stable than the (*S*,*S*) by 0.00739 energy units. The dipole moment of (*S*,*S*) is much larger than that of (*S*,*R*), the HOMO energy of (*S*,*R*) is lower than that of (*S*,*S*), the LUMO of (*S*,*R*) is higher than that of (S,S), and the HOMO-LUMO gap of (*S*,*R*) is wider than that of (*S*,*S*), indicating that the (*S*,*R*) isomer might also be more chemically stable, but also less reactive in terms of the electronic reactivity. The NMR shifts for ^{1}H and ^{13}C atoms also were obtained. We compare the experimental NMR chemical shifts with the calculated shifts for two diastereoisomers, (*S*,*S*) and (*S*,*R*), of compounds **1c**

and **1d** (Figure 3). By examining both hydrogen and carbon atoms, we aimed to determine which diastereoisomer more accurately reflected the experimental data. Upon examining the chemical shifts of compound **1c**, it is observed that the calculated values for the (*S*,*R*) diastereoisomer align more closely with the experimental data for most atoms. For H2, the hydrogen attached to the chiral center of the amino acid fragment, the (*S*,*S*) diastereoisomer, provides a better match with a value of 4.60 ppm compared to the experimental shift of 4.13 ppm. However, the (*S*,*R*) diastereoisomer showed greater consistency for other hydrogen atoms, such as H3b (the diastereotopic benzylic hydrogen atom of the amino acid fragment), H2a′ and H2b′ (the diastereotopic benzylic hydrogens of the dihydrochalcone moiety), and H3′ (the hydrogen attached to the chiral center of the dihydrochalcone fragment). Similarly, for the carbon atoms, the (*S*,*R*) diastereoisomer provides a closer match for key atoms such as C2′ (the benzylic carbon of the dihydrochalcone moiety) and C3 (the benzylic carbon of the amino acid fragment), whereas the (*S*,*S*) form better represents the chiral carbon of the amino acid fragment (C2) and the chiral carbon of the dihydrochalcone moiety (C3′). Despite this, the overall trend favored the (*S*,*R*) configuration for compound **1c**, as it offers more consistent alignment with the experimental values. A similar trend is observed in the analysis of compound **1d**. In both compounds, **1c** and **1d**, the (*S*,*R*) diastereoisomer shows a greater overall alignment with the experimental NMR chemical shifts. Although certain individuals shift, most of the hydrogen and carbon shifts favor the (*S*,*R*) configuration. Thus, based on this comparison, it seems that both compounds are more likely to exist in the (*S*,*R*) configuration under the conditions of the NMR experiments. This simulation established that the new chiral center with the *R* configuration must present a proton multiplet signal at around 5.26 ppm, whereas the one with the *S* configuration must present this signal at around 4.45 ppm. Thus, we concluded that the most abundant diastereoisomer corresponds to one with the (*S*,*R*) configuration, which was additionally enriched in the diastereomeric mixture after depuration by classic column chromatography due to the observed stability of the (*S*,*S*)-diastereoisomer.

The ^{13}C NMR spectra of compounds **1a**–**d** (Figures S3b–S6b) confirm the proposed structure. Given the presence of 23 different signals in the spectra, it is possible to affirm that the molecule only has symmetry in the ring with the presence of the substituent R=Cl, a 4-substituted system, showing only four signals for those carbon atoms that will appear in different chemical shifts. Between 14.0 and 61.0 ppm, the signals corresponding to the carbon atoms of the aliphatic part of the molecule appear, while, above 100 ppm, the different aromatic carbon atoms, and those with C=O and C=S bonds, appear. Specifically, the signals that appear most shifted in the spectra were assigned to the C=O groups of ketone and carboxylic acid ester, as well as to the C=S group of alkyl dithiocarbamate (between 170 and 205 ppm). Fully ^{1}H and ^{13}C atoms were achieved using HMQC, HMBC, COSY, and NOESY two-dimensional experiments for compound **1d** (Figure 4).

In the two-dimensional NMR experiments conducted on the compound under investigation, various types of hydrogen and carbon atoms were identified based on the correlations observed in the HMQC, HMBC, COSY, and NOESY spectra. The main findings are outlined below. The HMQC experiment identifies direct correlations between hydrogen and carbon atoms that are covalently bonded. Methyl group hydrogens at 1.30 ppm (triplet signal) are correlated with the methyl carbon atom of the ester fragment at 14.27 ppm. Methylene hydrogens, which appear as a multiplet at 4.48 ppm, are coupled with the methylene carbon of the ester fragment at 66.8 ppm. Hydrogen on the chiral carbon from the amino acid at 4.13 ppm correlates with the chiral carbon attached to the nitrogen at 61.7 ppm. Diastereotopic benzylic hydrogens from the amino acid fragment (δ_H = 3.39 and 3.41 ppm) are coupled to the benzylic carbon adjacent to the indole group (δ_C = 45.4 ppm), while the hydrogen atom on the chiral center in the dihydrochalcone fragment (δ_H = 5.24 ppm) correlates with the benzylic carbon adjacent to the 4-hydroxyphenyl group (δ_C = 58.3 ppm). Finally, benzylic hydrogens adjacent to the carbonyl group in the dihydrochalcone fragment, identified as the signals at 3.36 and 3.34 ppm, are coupled with carbon in position 2 relative to the ketone, identified as the signal at 27.1 ppm.

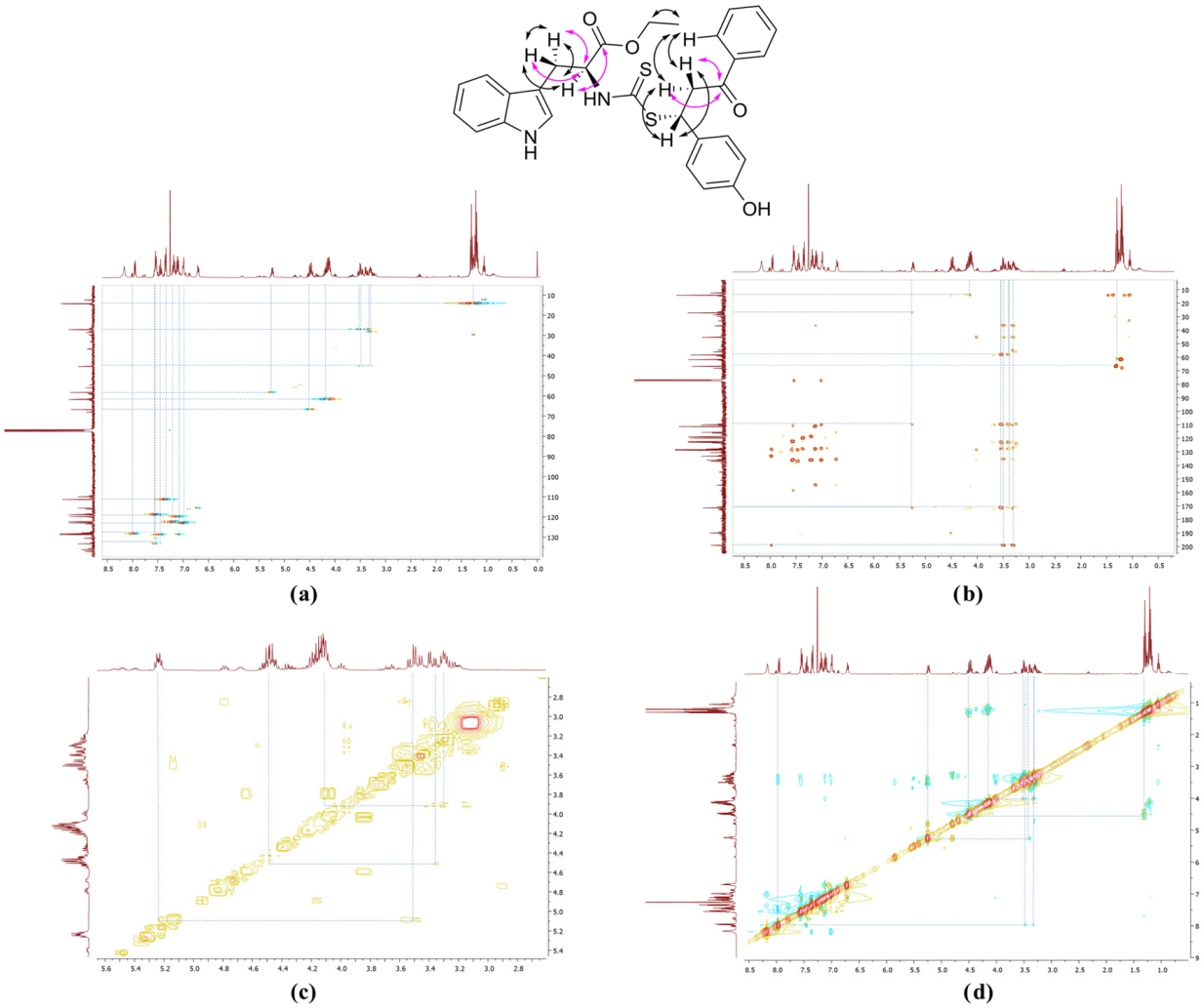

Figure 4. Two-dimensional NMR experiments for compound **1d**. (**a**) HMQC, (**b**) HMBC, (**c**) COSY, and (**d**) NOESY.

The HMBC, COSY, and NOESY experiments provided detailed insights into the structural and stereochemical relationships within compound **1d** through the observation of the long-range, scalar, and spatial correlations between hydrogens and carbons. The HMBC experiment revealed key long-range connections, such as the methyl hydrogens (δ_H = 1.30 ppm, triplet) being correlated with the methylene carbon of the ester group (δ_C = 66.8 ppm), and the chiral center hydrogen in the dihydrochalcone fragment (δ_H = 5.24 ppm, multiplet) showing correlations with several carbons, including carbon in position 2 relative to the ketone (δ_C = 27.1 ppm), the aromatic carbon in the 4-hydroxyphenyl ring (δ_C = 110 ppm), and the carbon of the C=S group in the dithiocarbamate fragment (δ_C = 171.5 ppm). The benzylic hydrogens adjacent to the carbonyl group in the dihydrochalcone fragment (δ_H = 3.36 and 3.34 ppm, multiplets) also showed correlations with the benzylic carbon adjacent to the 4-hydroxyphenyl group (δ_C = 58.3 ppm), the C=S carbon (δ_C = 171.5 ppm), and the C=O group (δ_C = 199.2 ppm).

In the COSY experiment, through-bond scalar couplings were identified, with the chiral center hydrogen in the dihydrochalcone fragment being coupled with the benzylic hydrogens adjacent to the carbonyl group, while the chiral carbon hydrogen from the amino acid fragment was coupled with the diastereotopic benzylic hydrogens (δ_H = 3.39 and 3.41 ppm, multiplets). The NOESY experiment provided information about spatial interactions, showing that the chiral center hydrogen in the dihydrochalcone fragment was spatially close to the benzylic hydrogens adjacent to the carbonyl group, and that the chiral

carbon hydrogen from the amino acid fragment was spatially close to the diastereotopic benzylic hydrogens. Additionally, the benzylic hydrogens adjacent to the carbonyl group were found to be spatially close to the hydrogen *orto* of the aryl fragment attached to the carbonyl group (δ_H = 7.95 ppm).

To carry out a complete characterization of the products obtained and to evaluate their chemical purity, compound **1a** was analyzed by GC-EIMS. The chromatogram of compound **1a** (Figure S7) showed three different major peaks with different retention times, a result that was unexpected given the resulting NMR profile. According to the respective mass spectra, the peaks were identified as a CH_2-type fragment, 1,3-diphenyl-3-sulfanylpropan-1-one type, and 2-isothiocyanate type, respectively. According to the results obtained by the CG-MS, it is possible to affirm that compound **1a** is thermolabile and undergoes cleavage reactions of the alkyl dithiocarbamate group in the GC injection port, given their high temperature. This behavior was found for all **1a**–**d** derivatives, which can be evidenced in the electronic impact mass spectra of each signal in the chromatogram. Efforts to measure the high-resolution mass spectra were unsuccessful, given the high reactivity of these derivatives in acidic media or the high temperatures.

Regarding the reaction that occurred for the formation of the **1a**–**d** derivatives, differences were found in the yields, which can be associated with the reaction conditions and structural considerations of the starting 4-substituted (*E*)-chalcones **3a**–**b** that determined the progress of the reaction. When the reactions were carried out for reaction times longer than 1 day, lower yields and a greater number of byproducts were established in all cases. The above demonstrates that the number of collateral reactions increases given the degradation of compounds **1a**–**d**, which are not as stable as the derivatives obtained by Quiroga [12,13]. Moreover, the yield values decrease when the electronic contribution of the substituents is greater, particularly when (*E*)-chalcones present electron donor groups in the 4-position. The presence of electron-withdrawing groups, such as -Cl, improves their electrophilicity, favoring the Michael addition reaction of the respective intermediate dithiocarbamate ion. In general terms, the formation of compounds of the **1a**–**d** type presented moderate-to-low yield percentages compared to the analogs previously obtained of the vinyl ketone type [12–14], presumably due to the steric hindrance involved in the Michael addition reaction stated for the reaction mechanism.

Once the characterization and the target compounds were achieved, biological tests were carried out on them against the phytopathogen *F. oxysporum*. These tests included the chalcone precursors **3a**–**b** and the compounds **1a**–**d**. Table 2 presents the IC_{50} values for the evaluated compounds. Compound **3b** has a much lower IC_{50} value (0.06 mM) than compound **3a** (9.63 mM). This indicates that the presence of a *para*-hydroxyl group is significantly more effective in inhibiting the growth of *F. oxysporum* than the presence of a chlorine atom at the same position.

Table 2. Measured IC_{50} values for compounds **1a**–**d** and precursors **3a**–**b** against *Fusarium oxysporum*.

Compound	1a	1b	1c	1d	3a	3b
IC_{50} (mM)	5.71	1.46	0.33	1.12	9.63	0.06

When comparing the dithiocarbamate-type compounds **1a** and **1b**, which are derived from **3a** but differ in the L-tryptophan ester used, compound **1a** has an IC_{50} of 5.71 mM, while **1b** has an IC_{50} of 1.46 mM. This outcome suggests that the alkyl ester moiety affects the inhibitory activity. Thus, the L-tryptophan ethyl ester improves the inhibitory activity against *F. oxysporum* compared to the methyl ester. Regarding **1c** and **1d**, both compounds are derived from **3b** and differ in the L-tryptophan ester used, suggesting that the tryptophan methyl ester appears to be more effective than the ethyl ester when combined with **3b**. In general, the ethyl ester appears to be more effective than the methyl ester when combined with base compound **3a**, but this trend is reversed with base compound **3b**. From the other perspective, compounds derived from **3b** (**1c** and **1d**) have lower IC_{50} values

than those derived from **3a** (**1a** and **1b**). This fact reinforces the idea that a hydroxyl group at position 4 (as in **3b**) significantly enhances the inhibitory activity against *F. oxysporum*. These results are comparable to that of the IC_{50} value of the positive control fludioxonil (i.e., 0.061 mM), a synthetic phenylpyrrole used commercially as a non-systemic fungicide. Overall, the above findings established that the modification at the 4-position of the base compound has a significant impact on the inhibitory activity. The hydroxyl group in **3b** seems to be more effective than the chlorine atom in **3a**. The most effective compound in this series is **3b**, with an IC_{50} of 0.06 mM, followed by **1c**, with an IC_{50} of 0.33 mM. This suggests that modifications that include a hydroxyl group at position 4 are promising for future research and the optimization of inhibitory compounds against *F. oxysporum*.

These findings can be contextualized within the existing literature on antifungal agents. For instance, various studies have reported that compounds with IC_{50} values in the low micromolar range (typically < 1 mM) are considered effective against *Fusarium* species [32], such as fludioxonil, but lesser than azole-containing antifungals having an IC_{50} < 0.1 mM [33]. The observed IC_{50} values of compounds **1c** and **1d** align well with this criterion, indicating their potential as lead compounds in antifungal development under structural optimization. However, the disparity in activity among the test compounds, particularly the significant increased potency for **1c**, underscores the importance of structural optimization in developing effective antifungal agents, particularly the introduction of a 4-hydroxyphenyl moiety in the (*E*)-chalcone precursor and a methyl ester in the L-tryptophanate fragment. Hence, future studies will be focused on elucidating the specific mechanisms underlying the enhanced activity of these compounds, potentially through in vitro efficacy assessments against various *Fusarium* species, to further establish their therapeutic relevance.

Several chiral pesticides, including fungicides, have been commercially launched as diastereomeric mixtures [34]. In this regard, although the target compounds **1a**–**d** were also evaluated as diastereomeric mixtures (*S*,*S*/*S*,*R*), it is important to consider that these mixtures may have a different impact on the biological activity than the individual diastereomers. Despite having the same molecular formula, diastereomers have different spatial arrangements of atoms, which can lead to varying interactions with biological targets [35]. For instance, one diastereomer may fit better into the active site of an enzyme, enhancing its antifungal activity, while another may have little to no effect. In addition, each diastereomer in a mixture may exhibit different IC_{50} values, and this variability can influence the overall potency of the mixture. If one diastereomer is much more effective than the other, it can skew the perceived effectiveness of the mixture, as reported for chiral antifungals [36]. However, in some cases, the presence of multiple diastereomers can result in concomitant, synergistic, or antagonistic effects, where the combined activity of the diastereomers can be greater or lower than the sum of their individual effects [37,38]. Particularly, a diastereomerically mediated synergistic effect can also impact positively on resistance, since the presence of multiple diastereomers could potentially slow down the development of resistance, as the fungus may not be able to adapt to all forms simultaneously [39]. Other aspects, such as the toxicity, pharmacokinetics and pharmacodynamics, and stability, can vary depending on the diastereoisomeric nature of the bioactive [40]. Therefore, understanding the impact of diastereomeric mixtures on the antifungal activity is essential for optimizing the efficacy of antifungal agents. It can help guide the design of new compounds, their formulation, and their application in clinical or field settings. Comprehensive studies that investigate the individual contributions of diastereomers to the antifungal activity could pave the way for more effective and targeted treatments against fungal infections. This exploration can be pursued in future research.

4. Concluding Remarks

The present study demonstrated the synthesis and characterization of 4-substituted (*E*)-chalcone derivatives, leading to the formation of the L-tryptophan-derived dithiocarbamate compounds **1a**–**d**. The synthesis involved a two-stage methodology under microwave

irradiation, combining the alkyl ester preparation from L-tryptophan and subsequent three-compound condensation. The yields for the products **1a–d** were moderate to high, with values ranging from 56 to 76% and diastereomeric excess from 6.8 to 14.2%. Comprehensive characterization through NMR and GC-EIMS confirmed the structures and provided insights into their stability and potential diastereoisomers. Antifungal testing against the phytopathogen *F. oxysporum* revealed significant inhibitory activity, especially for compounds derived from the 4-hydroxychalcone. Notably, compound **3b** exhibited an IC_{50} of 0.06 mM, significantly outperforming its chlorine-substituted counterpart (**3a**). Among the dithiocarbamate derivatives, **1c** (derived from **3b** with a tryptophan methyl ester) showed the highest activity, with an IC_{50} of 0.33 mM. These findings highlight the critical role of substituents at the 4-position of chalcones and the ester type in determining the antifungal activity. This study suggests that further modifications, particularly those incorporating a hydroxyl group at position 4, could enhance the efficacy of chalcone-based inhibitors against *F. oxysporum*. Future research should focus on optimizing these structural features to develop more potent antifungal agents.

Supplementary Materials: The following supporting information can be downloaded at: https://www.mdpi.com/article/10.3390/org5040031/s1, Figure S1. ^{1}H NMR experiments of the reaction crude of compound **1a**; Figure S2. ^{1}H and ^{13}C NMR experiments of compound (*S*,*S*)-**1a**; Figure S3. ^{1}H and ^{13}C NMR experiments of compound (*S*,*R*)-**1a**; Figure S4. ^{1}H and ^{13}C NMR experiments of compound (*S*,*R*)-**1b**; Figure S5. ^{1}H and ^{13}C NMR experiments of compound (*S*,*R*)-**1c**; Figure S6. ^{1}H and ^{13}C NMR experiments of compound (*S*,*R*)-**1d**; Figure S7. GC-EIMS analysis of compound (*S*,*R*)-**1a**; Figure S8. MS-ESI(+) spectra of compounds **1a–d**; Figure S9. Dose–response curves of compounds **1a–d** against *Fusarium oxysporum*.

Author Contributions: Conceptualization, E.C.-B., I.B. and D.Q.; methodology, E.C.-B., I.B. and D.Q.; software, E.C.-B. and D.Q.; investigation, N.A.-I. and S.T.-C.; resources, E.C.-B. and D.Q.; writing—original draft preparation, E.C.-B. and D.Q.; writing—review and editing, S.T.-C., E.C.-B. and D.Q.; project administration, E.C.-B. and D.Q.; funding acquisition, E.C.-B. and D.Q. All authors have read and agreed to the published version of the manuscript.

Funding: This study was granted by the Universidad Militar Nueva Granada (UMNG). It is a product derived from the project INV-CIAS-2043, funded by Vicerrectoría de Investigaciones at UMNG–Validity 2016.

Data Availability Statement: The data presented in this study are available on request from the corresponding author.

Acknowledgments: The authors thank UMNG for funding this study.

Conflicts of Interest: The authors declare no conflicts of interest.

References

1. Azizi, N.; Aryanasab, F.; Saidi, M.R. Straightforward and Highly Efficient Catalyst-Free One-Pot Synthesis of Dithiocarbamates under Solvent-Free Conditions. *Org. Lett.* **2006**, *8*, 5275–5277. [CrossRef] [PubMed]
2. Ajiboye, T.O.; Ajiboye, T.T.; Marzouki, R.; Onwudiwe, D.C. The Versatility in the Applications of Dithiocarbamates. *Int. J. Mol. Sci.* **2022**, *23*, 1317. [CrossRef] [PubMed]
3. Ivanov, A.V.; Loseva, O.V.; Rodina, T.A. Chemisorptive Synthesis, Self-Assembly of Complicated 2D and 3D Supramolecular Architectures (Role of Hydrogen Bonds and Secondary Interactions Au···S and S···Cl), and Thermal Behavior of Pseudo-Polymeric Gold(III)–Mercury(II) Dibutyldithiocarbamato-Chlorido Complexes. *Russ. J. Coord. Chem.* **2020**, *46*, 639–652. [CrossRef]
4. Chen, C.; Zhang, L.-S.; Qian, Z.; Jia, A.-Q.; Zhang, Q.-F. Synthesis, Structural Characterization and Photocatalytic Water-Oxidation Properties of Mononuclear Bis(o-Phenanthroline) Ruthenium(II) Complexes with Dithiocarbamate Ligands. *J. Mol. Struct.* **2021**, *1233*, 130078. [CrossRef]
5. Scozzafava, A.; Mastrolorenzo, A.; Supuran, C.T. Arylsulfonyl-N,N-Dialkyl-Dithiocarbamates as Tumor Cell Growth Inhibitors: Novel Agents Targeting β-Tubulin? *J. Enzym. Inhib.* **2001**, *16*, 55–63. [CrossRef]
6. Altaf, M.; Monim-ul-Mehboob, M.; Seliman, A.A.A.; Sohail, M.; Wazeer, M.I.M.; Isab, A.A.; Li, L.; Dhuna, V.; Bhatia, G.; Dhuna, K. Synthesis, Characterization and Anticancer Activity of Gold(I) Complexes That Contain Tri-Tert-Butylphosphine and Dialkyl Dithiocarbamate Ligands. *Eur. J. Med. Chem.* **2015**, *95*, 464–472. [CrossRef]
7. Mehta, R.G.; Liu, J.; Constantinou, A.; Thomas, C.F.; Hawthorne, M.; You, M.; Gerhäuser, C.; Pezzuto, J.M.; Moon, R.C.; Moriarty, R.M. Cancer Chemopreventive Activity of Brassinin, a Phytoalexin from Cabbage. *Carcinogenesis* **1995**, *16*, 399–404. [CrossRef]

8. Gaspari, P.; Banerjee, T.; Malachowski, W.P.; Muller, A.J.; Prendergast, G.C.; DuHadaway, J.; Bennett, S.; Donovan, A.M. Structure−Activity Study of Brassinin Derivatives as Indoleamine 2,3-Dioxygenase Inhibitors. *J. Med. Chem.* **2006**, *49*, 684–692. [CrossRef]
9. Lee, J.H.; Kim, C.; Sethi, G.; Ahn, K.S. Brassinin Inhibits STAT3 Signaling Pathway through Modulation of PIAS-3 and SOCS-3 Expression and Sensitizes Human Lung Cancer Xenograft in Nude Mice to Paclitaxel. *Oncotarget* **2015**, *6*, 6386–6405. [CrossRef]
10. Banerjee, T.; DuHadaway, J.B.; Gaspari, P.; Sutanto-Ward, E.; Munn, D.H.; Mellor, A.L.; Malachowski, W.P.; Prendergast, G.C.; Muller, A.J. A Key in Vivo Antitumor Mechanism of Action of Natural Product-Based Brassinins Is Inhibition of Indoleamine 2,3-Dioxygenase. *Oncogene* **2008**, *27*, 2851–2857. [CrossRef]
11. Sellam, A.; Iacomi-Vasilescu, B.; Hudhomme, P.; Simoneau, P. In Vitro Antifungal Activity of Brassinin, Camalexin and Two Isothiocyanates against the Crucifer Pathogens *Alternaria Brassicicola* and *Alternaria Brassicae*. *Plant Pathol.* **2007**, *56*, 296–301. [CrossRef]
12. Quiroga, D.; Becerra, L.; Sadat-Bernal, J.; Vargas, N.; Coy-Barrera, E. Synthesis and Antifungal Activity against Fusarium Oxysporum of Some Brassinin Analogs Derived from L-Tryptophan: A DFT/B3LYP Study on the Reaction Mechanism. *Molecules* **2016**, *21*, 1349. [CrossRef] [PubMed]
13. Quiroga, D.; Becerra, L.D.; Coy-Barrera, E. Ultrasound-Assisted Synthesis, Antifungal Activity against *Fusarium Oxysporum*, and Three-Dimensional Quantitative Structure–Activity Relationship of *N*,*S*-Dialkyl Dithiocarbamates Derived from 2-Amino Acids. *ACS Omega* **2019**, *4*, 13710–13720. [CrossRef] [PubMed]
14. Narwal, S.; Devi, B.; Dhanda, T.; Kumar, S.; Tahlan, S. Exploring Chalcone Derivatives: Synthesis and Their Therapeutic Potential. *J. Mol. Struct.* **2024**, *1303*, 137554. [CrossRef]
15. Angarita-Rodríguez, A.; Quiroga, D.; Coy-Barrera, E. Indole-Containing Phytoalexin-Based Bioisosteres as Antifungals: In Vitro and In Silico Evaluation against Fusarium Oxysporum. *Molecules* **2019**, *25*, 45. [CrossRef]
16. Vasudha, D.; Jagadeesh, A.; Konidala, S.K.; Yasin, H.; Mali, S.N.; Bhandare, R.R.; Shaik, A.B. Development of Orally Active Anti-Inflammatory Agents: In Vivo and In Silico Analysis of Naphthalene-Chalcone Derivatives Based on 2-Acetyl-6-Methoxy Naphthalene. *Chem. Phys. Impact* **2024**, *8*, 100472. [CrossRef]
17. Zhan, W.; Zhou, R.; Mao, P.; Yuan, C.; Zhang, T.; Liu, Y.; Tian, J.; Wang, H.; Xue, W. Synthesis, Antifungal Activity and Mechanism of Action of Novel Chalcone Derivatives Containing 1,2,4-Triazolo-[3,4-b]-1,3,4-Thiadiazole. *Mol. Divers.* **2024**, *28*, 461–474. [CrossRef]
18. Shah, A.; Desai, K.; Bhanusali, A.; Malek, N.; Naik, N.; Thakar, A.; Shah, A. Molecular Modelling, Cytotoxicity & Biological Investigation of Novel Fluorinated Diphenylamine Chalcone Derivatives. *J. Mol. Struct.* **2024**, *1311*, 138379. [CrossRef]
19. Zhang, T.; Liu, Y.; Xin, H.; Tian, J.; Deng, T.; Meng, K.; An, Y.; Xue, W. Synthesis and Antifungal Activity of Chalcone Derivatives Containing 1,3,4-Thiadiazole. *Chem. Biodivers.* **2024**, *21*, e202401031. [CrossRef]
20. Qian, W.; Lu, J.; Gao, C.; Liu, Q.; Li, Y.; Zeng, Q.; Zhang, J.; Wang, T.; Chen, S. Deciphering Antifungal and Antibiofilm Mechanisms of Isobavachalcone against Cryptococcus Neoformans through RNA-Seq and Functional Analyses. *Microb. Cell Factories* **2024**, *23*, 107. [CrossRef]
21. Marentes-Culma, R.; Orduz-Díaz, L.; Coy-Barrera, E. Targeted Metabolite Profiling-Based Identification of Antifungal 5-n-Alkylresorcinols Occurring in Different Cereals against Fusarium Oxysporum. *Molecules* **2019**, *24*, 770. [CrossRef] [PubMed]
22. Andrés Coy-Barrera, C.; Camilo Monge, I.; Quiroga, D. Non-Soluble Chalcones and Their Potential Application as Corrosion Coatings on Carbon Steel Exposed to 1 M HCl Solutions. *Arab. J. Chem.* **2023**, *16*, 104459. [CrossRef]
23. Li, J.; Sha, Y. A Convenient Synthesis of Amino Acid Methyl Esters. *Molecules* **2008**, *13*, 1111–1119. [CrossRef] [PubMed]
24. Kenari, F.; Molnár, S.; Perjési, P. Reaction of Chalcones with Cellular Thiols. The Effect of the 4-Substitution of Chalcones and Protonation State of the Thiols on the Addition Process. Diastereoselective Thiol Addition. *Molecules* **2021**, *26*, 4332. [CrossRef] [PubMed]
25. Mehta, K.; Wani, A.A.; Bharatam, P.V. Phospha-Michael Addition of Biphenylphosphine Oxide to Chalcones and α,β-Unsaturated Esters Using the Organocatalyst 1,1-Diaminobenzalazine. *Tetrahedron Lett.* **2023**, *122*, 154505. [CrossRef]
26. Sherzad Othman, S.; Noori Abdullah, M. Synthesis of Novel Michael Adducts and Study of Their Antioxidant and Antimicrobial Activities. *Chem. Rev. Lett.* **2022**, *5*, 226–233. [CrossRef]
27. Al-Jaber, N.A.; Bougasim, A.S.A.; Karah, M.M.S. Study of Michael Addition on Chalcones and or Chalcone Analogues. *J. Saudi Chem. Soc.* **2012**, *16*, 45–53. [CrossRef]
28. Minsat, L.; Peyrot, C.; Brunissen, F.; Renault, J.-H.; Allais, F. Synthesis of Biobased Phloretin Analogues: An Access to Antioxidant and Anti-Tyrosinase Compounds for Cosmetic Applications. *Antioxidants* **2021**, *10*, 512. [CrossRef]
29. Venianakis, T.; Oikonomaki, C.; Siskos, M.G.; Varras, P.C.; Primikyri, A.; Alexandri, E.; Gerothanassis, I.P. DFT Calculations of 1H- and 13C-NMR Chemical Shifts of Geometric Isomers of Conjugated Linoleic Acid (18:2 ω-7) and Model Compounds in Solution. *Molecules* **2020**, *25*, 3660. [CrossRef]
30. Venianakis, T.; Oikonomaki, C.; Siskos, M.G.; Primikyri, A.; Gerothanassis, I.P. DFT Calculations of 1H NMR Chemical Shifts of Geometric Isomers of Conjugated Linolenic Acids, Hexadecatrienyl Pheromones, and Model Triene-Containing Compounds: Structures in Solution and Revision of NMR Assignments. *Molecules* **2021**, *26*, 3477. [CrossRef]
31. Safi, Z.S.; Wazzan, N. DFT Calculations of 1H- and 13C-NMR Chemical Shifts of 3-Methyl-1-Phenyl-4-(Phenyldiazenyl)-1H-Pyrazol-5-Amine in Solution. *Sci. Rep.* **2022**, *12*, 17798. [CrossRef] [PubMed]

32. Borrego-Muñoz, P.; Coy-Barrera, E.; Quiroga, D. New Strategies in the Chemical Control of *Fusarium Oxysporum* UsingSynthetic Bioisosteres of Secondary Metabolites: A Review of the SyntheticMethods for Novel Compounds with Potential Antifungal Activity. *Mini-Rev. Org. Chem.* **2024**, *21*, 794–810. [CrossRef]
33. Teixeira, M.M.; Carvalho, D.T.; Sousa, E.; Pinto, E. New Antifungal Agents with Azole Moieties. *Pharmaceuticals* **2022**, *15*, 1427. [CrossRef] [PubMed]
34. Jeschke, P. Current Status of Chirality in Agrochemicals. *Pest Manag. Sci.* **2018**, *74*, 2389–2404. [CrossRef] [PubMed]
35. Scott, K.A.; Ropek, N.; Melillo, B.; Schreiber, S.L.; Cravatt, B.F.; Vinogradova, E.V. Stereochemical Diversity as a Source of Discovery in Chemical Biology. *Curr. Res. Chem. Biol.* **2022**, *2*, 100028. [CrossRef]
36. Shi, W.; Nacev, B.A.; Bhat, S.; Liu, J.O. Impact of Absolute Stereochemistry on the Antiangiogenic and Antifungal Activities of Itraconazole. *ACS Med. Chem. Lett.* **2010**, *1*, 155–159. [CrossRef]
37. Melillo, B.; Zoller, J.; Hua, B.K.; Verho, O.; Borghs, J.C.; Nelson, S.D.; Maetani, M.; Wawer, M.J.; Clemons, P.A.; Schreiber, S.L. Synergistic Effects of Stereochemistry and Appendages on the Performance Diversity of a Collection of Synthetic Compounds. *J. Am. Chem. Soc.* **2018**, *140*, 11784–11790. [CrossRef]
38. Mallebrera, B.; Brandolini, V.; Font, G.; Ruiz, M.J. Cytoprotective Effect of Resveratrol Diastereomers in CHO-K1 Cells Exposed to Beauvericin. *Food Chem. Toxicol.* **2015**, *80*, 319–327. [CrossRef]
39. Guin, S.; Alden, K.M.; Krysan, D.J.; Meyers, M.J. Synthesis and Antifungal Activity of Stereoisomers of Mefloquine Analogs. *ACS Med. Chem. Lett.* **2024**, *15*, 822–827. [CrossRef]
40. Terekhov, R.P.; Savina, A.D.; Pankov, D.I.; Korochkina, M.D.; Taldaev, A.; Yakubovich, L.M.; Zavadskiy, S.P.; Zhevlakova, A.K.; Selivanova, I.A. Insights into the Stereoisomerism of Dihydroquercetin: Analytical and Pharmacological Aspects. *Front. Chem.* **2024**, *12*, 1439167. [CrossRef]